Cancer Cell International

RESEARCH

Open Access

Gr-1 blockade remodels the immunosuppressive microenvironment induced by incomplete microwave ablation of hepatocellular carcinoma

Tian Huang[1,5†], Hensong Cao[2†], Shipeng Dai[1†], Yonghua Zhu[1], Hanyuan Liu[2], Shuxian Zhu[3], Zhengqing Lu[1], Chuan Liu[1], Chengyu Lv[2*], Zhouxiao Li[4*], Jinhua Song[1*] and Han Zhuo[1*]

Abstract

Background Ablation is one of the main methods for local treatment of hepatocellular carcinoma (HCC). Different from radiofrequency ablation (RFA), microwave ablation (MWA) is not limited by tissue conductivity, and can use multiple electrodes at the same time to improve ablation efficiency. In addition, MWA can form a larger ablation area, which makes it possible to completely ablate large HCC. However, MWA may be incomplete due to factors such as larger tumors or tumors in high-risk areas. The mechanism by which the cellular and tumor immune microenvironment (TIME) is involved in the in vitro effects of incomplete microwave ablation (iMWA) needs to be further elucidated.

Methods H22 tumor-bearing C57BL/6 mice were treated with iMWA with several combinations of ablation power and time duration. The effects of iMWA on the genes of HCC cancer cells and the TIME were investigated by RNA sequencing, mass cytometry, immunohistochemistry, and immunofluorescence. The effect of iMWA in combination with anti-Gr-1 on HCC tumor growth was also evaluated.

Results Thermal stress generated by iMWA induced coagulative necrosis and apoptosis in the region of the ablation center of HCC. RNA sequencing analysis showed that iMWA can boost chemokine CXCL5, which was further confirmed by quantitative real time polymerase chain reaction (qRT-PCR). Mass cytometry results showed that relative to Ctrl group, iMWA-treated led to decreased $CD4^+$ T, $CD8^+$ T, Natural killer (NK), macrophages including both M1 and M2 types but increased monocytes and bone marrow-derived suppressor cells (MDSC). Therefore, inhibiting MDSC is the main target in the later stage of iMWA. In vivo results showed that the tumor volume and weight of iMWA+ anti-Gr-1 group were significantly reduced compared with iMWA+ anti-IgG group. In addition,

†Tian Huang, Hensong Cao and Shipeng Dai contributed equally.

*Correspondence:
Chengyu Lv
lcy_1234@aliyun.com
Zhouxiao Li
liizhouxiao1991@outlook.com
Jinhua Song
jinhuasongnanj@163.com
Han Zhuo
han12175@hotmail.com
Full list of author information is available at the end of the article

the merged expressions of CD11b and Gr-1 proteins were found reduced in the iMWA+ anti-Gr-1 group compared with the iMWA+ anti-IgG group by immunofluorescence staining. Immunohistochemistry suggested that CD8 was enriched in the iMWA+ anti-Gr-1 group but not in the iMWA+ anti-IgG group.

Conclusion Our data suggests that iMWA and Gr-1 blocking combined therapy can further inhibit HCC growth and significantly improve the $CD8^+$ T cells in the mouse subcutaneous tumor model, which brings good news to HCC patients.

Keywords Microwave ablation, Gr-1, Cancer immunotherapy, Bone marrow-derived suppressor cells, Hepatocellular carcinoma

Introduction

Hepatocellular carcinoma (HCC) is one of the most common malignant tumors of digestive system, with the sixth incidence and the second mortality [1, 2]. In general, the prognosis of HCC is poor, the ratio of morbidity to mortality reaches 1:0.9, which seriously endangers people's life and health. Like most malignant tumor of digestive system, surgery is still the best treatment for resectable HCC [3–5]. However, many prospective and retrospective studies have confirmed that the 5-year survival rate of local ablation for early small HCC is close to 60%. There was no significant difference in the survival rate between local ablation and surgical resection in this group of patients [6–8]. Therefore, local ablation is an important treatment for patients with small HCC who are not suitable for surgical treatment.

Under the guidance of ultrasound, computer tomography (CT) or Magnetic Resonance Imaging (MRI), local ablation can cause coagulation necrosis of tumor by physical or chemical methods, so as to achieve the purpose of local eradication of tumor. Radiofrequency ablation (RFA) is the most widely used local ablation technique for HCC. The principle of RFA therapy is that the head end of the radio frequency therapeutic electrode inserted into the tumor tissue emits radio frequency current, and then excites the tissue cells around the electrode to carry out ion oscillation, which making the intracellular temperature of the tumor tissue exceed 60 °C, High temperature causes irreversible necrosis of cells, coagulates blood vessels around tumors and blocks blood supply to tumors [7, 9]. Different from RFA, microwave ablation (iMWA) is not limited by tissue conductivity, and can use multiple electrodes at the same time to improve ablation efficiency. In addition, MWA can form a larger ablation area, which makes it possible to completely ablate large HCC [10–12]. Cryoablation relies on freezing temperature to induce tumor cell death, which is the earliest local ablation technique for effective treatment of benign and malignant liver tumors [13, 14]. It can be seen that local ablation therapy not only has the curability of surgical resection, but also has its unique minimally invasive and cost-effective.

The efficiency of MWA in treating HCC is clearly limited by incomplete ablation of large tumors and tumors at high-risk sites. However, until now, few studies have explored the effect of incomplete MWA (iMWA) on tumor immune microenvironment (TIME) in HCC. Tumor immune microenvironment (TIME) include tumor cells, immune cells, cytokines, etc. The interactions between these components, which are divided into anti-tumor and pro-tumor, determine the trend of anti-tumor immunity. Although the immune system can eliminate tumor through the cancer-immune cycle, tumors appear to eventually evade from immune surveillance by shaping an immunosuppressive microenvironment [15, 16]. Immunotherapy reshapes the TIME and restores the tumor killing ability of anti-tumor immune cells. In the present study, the effects of iMWA on the genes of HCC cancer cells and the tumor microenvironment were investigated by RNA sequencing, mass cytometry, immunohistochemistry, and immunofluorescence. The goal of our study is to provide theoretical possibilities for a new protocol for patients with giant HCC, namely iMWA combined with immunotherapy.

Materials and methods

Cell cultures

We procured mouse HCC cell line H22 from the Chinese Academy of Sciences Type Culture Bank. H22 were then grown in RIPA 1640 medium (Gibco, USA) supplemented with 10% fetal bovine serum and 1% penicillin/streptomycin. The culturing of these cells was maintained at a steady temperature of 37 °C with a 5% CO2 environment in a temperature-controlled incubator.

In vivo tumor mice model and iMWA treatment

The Nanjing Medical University Animal Management Committee gave its approval for the animal experiment, and all experimental techniques and animal care adhered to the institutional ethical standards for animal-related investigations. The Nanjing Medical University Laboratory Animal Centre used specialised pathogen-free (SPF) breeding practise to raise all of its mice. The cervical dislocation used to sacrifice mice.

C57BL/6 wild-type mice were bought from the Nanjing Medical University Model Animal Research Centre. Before tumour implantation, all animals were examined to make sure they were healthy and free of illness. C57BL/6 mice received subcutaneous injections of H22 cells. Four groups were created from the tumour model mice with transplanted carcinomas, Ctrl (no treatment), iMWA, iMWA+ anti-IgG, iMWA+ anti-Gr-1, each group had 5 mice. When the tumors grew into 150–200 mm^3 in volume, iMWA, iMWA+ anti-IgG and iMWA+ anti-Gr-1 group received incomplete ablation. One week after ablation, 10 mg/kg anti-IgG or anti-Gr-1 (MedChemExpress, Shanghai, China) was intraperitoneal injected into the mice in iMWA+ anti-IgG and iMWA+ anti-Gr-1 groups, and once a week. The tumor size was measured every 3 days and the tumor volume was calculated using the following formula: volume $(mm^3) = width^2 \times length/2$.

iMWA treatment

When the original tumor reached 150–200 mm^3, it was treated with MWA utilizing a microwave generator (KY-2000, Canyon Medical, Nanjing, China) Intraperitoneal injection of avertin (1.25% avertin, EasyCheck, Nanjing AIBI Bio-Technology Co. Ltd., M2910) was used to anesthetize mice. After inserting a MWA antenna (KY-2450A-1, Canyon Medical, Nanjing, China) into the primary tumor's center, several powers and timings of iMWA treatment were used. In our investigations, we employed a microwave radiation frequency of 2450 MHz for 15 s.

RNA sequencing

Mice tumors from iMWA treatment and control were lysed in Trizol and then subjected to RNA sequencing. The total amount of RNA used as input material for the RNA sample preparations was 2 μg RNA per sample. Using the Illumina VAHTS mRNA-seq v2 Library Prep Kit, sequencing libraries were produced. index codes were applied to each sample in accordance with the manufacturer's recommendations in order to assign sequences to it. In short, poly-T oligo-attached magnetic beads were used to separate mRNA from total RNA. Fragmentation buffer was used during the process. After first strand cDNA synthesis, second strand cDNA synthesis was carried out. The leftover overhangs were made into blunt ends. DNA fragments with their 3′ ends adenylated were ligated using an adapter with a hairpin loop shape. Next, the Polymerase Chain Reaction (PCR) was carried out. Finally, a final library size of roughly 350 bp was achieved by Qubit HS quantification and Agilent 2100 Bioanalyzer/Fragment Analyzer 5300 quality control. Following the manufacturer's instructions, the libraries were sequenced on an Illumina NovaSeq platform to produce 150 bp paired-end reads (Berry Genomics, Beijing, China).

Bioinformatic analysis

RNAs differential expression analysis was performed by DESeq2 software between two different groups. The genes with the parameter of false discovery rate (FDR) ≤ 0.05 and $|\text{Fold change}| \geq 2$ were considered differentially expressed genes. All DEGs were mapped to GO terms in the Gene Ontology database (http://www.geneontology.org/), gene numbers were calculated for every term, significantly enriched GO terms in DEGs comparing to the genome background were defined by hypergeometric test. FDR ≤ 0.05 was used as the threshold for the calculated p-value. GO terms meeting this condition were defined as significantly enriched GO terms. KEGG pathway enrichment analysis identified significantly enriched metabolic pathways or signal transduction pathways in DEGs comparing with the whole genome background. The calculating formula and filtering rules are the same as for the GO analysis. The Gene Ontology gene sets (c5.go.bp.v7.4.symbols) gene set was used for the enrichment analysis in GSEA v 4.3.0 software (https://www.gsea-msigdb.org/gsea/index.jsp). The genes identified to be on the leading edge of the enrichment profile were subject to pathway analysis. The normalized enrichment score (NES) is the primary statistic for examining gene set enrichment results. The nominal P value estimates the statistical significance of the enrichment score. A gene set with nominal $P \leq 0.05$ was considered to be significantly enriched in genes.

RNA extraction and quantificational real-time polymerase chain reaction (qRT-PCR)

We utilized the FastPure® Cell/Tissue Total RNA Isolation Kit V2 (Vazyme, China) to extract total RNA from cells and samples as per the provided instructions by the manufacturer. By employing a reverse transcription kit (Vazyme, China), the RNA was transcribed in reverse into cDNA. The specific sequences of each primer are presented in Table S1. In order to establish normalized mRNA expression levels, we used GAPDH as a reference.

ELISA

The evaluation of CXCL5 was conducted utilizing a CXCL5 ELISA kit commercially procured from Meimian biotechnology, China. The assays were in compliance with the protocols stipulated by the kit manufacturer. Subsequent analysis was executed through a microplate reader, quantifying the sample's absorbance (OD) at a wavelength of 450 nm.

Immunofluorescence and immunohistochemistry

Immunofluorescent cells were fixed with 4% Paraformaldehyde (Generalbiol, China) for a period of 20 min under ambient conditions, followed by cell permeabilization for 10 min using 0.05% Triton X-100 (Sigma-Aldrich, USA). The specimens were then blocked using PBS that contained 2% BSA and left to stand for 60 min at room temperature, following which they were incubated at 4 °C throughout the night with specific antibodies for CD11b, Gr-1, TUNEL, Ki67 (Bioss, China). Further, these samples underwent an additional 60-min incubation at room temperature with either Alexa Fluor or HRP-linked secondary antibodies (Abcam, UK). Nuclei were counterstained with Hoechst 33342 (Sigma-Aldrich, USA) and visuals were captured via laser scanning confocal microscopy. In terms of immunohistochemistry studies, the samples were kept overnight at 4 °C with antibodies targeting CD8 (Bioss, China) and immune responses were detected the following day using 3′-diaminobenzidine (DAB) (Generalbiol, China), in line with the supplier's guidelines.

Mass cytometry

We obtained tissue samples from MWA treatment and control tumor-bearing groups. We then processed mouse tumor tissue using the Miltenyi Mouse Tumor Isolation Kit (Miltenyi Biotec, Germany), in which Percoll removes debris and divides red blood cells. More experimental details refer to our previous research work [17].

Statistical analysis

Data were shown as the mean ± standard deviation (SD). Graphpad Prism 8.0 was utilized as the primary tool for performing the bulk of the analytical tasks in this study, where a p-value of less than or equal to 0.05 was considered indicative of statistical significance. Independent t-tests were deployed for comparative analyses across the various groups within the study.

Results

Thermal stress induces cell necrosis and apoptosis in the central region of iMWA in HCC

To assess the effect of iMWA on HCC, we established a subcutaneous tumor bearing model of C57BL/6 mice using H22 cells. iMWA (~ 50% ablation) treatment was performed 2 weeks after tumor inoculation and sham surgery was performed in Ctrl group (Fig. 1A). H&E staining indicated that the areas of coagulative necrosis in tumor tissues of iMWA (Fig. 1B). In addition, immunofluorescence also confirmed that iMWA induced apoptosis in a large number of HCC cells in the central ablation area (Fig. 1C). The above data confirm that thermal stress generated by iMWA induces coagulative necrosis and apoptosis in the region of the ablation center of HCC.

iMWA boosts chemokines based on RNA sequencing analysis in HCC mice model

But what is the effect of iMWA on the genetic level in HCC tissues? To confirm this, we used tumor tissues from Ctrl and iMWA group for RNA-sequencing in order to examine the potential molecular processes. Differential genes are visible on volcano map (Fig. 2A). In the iMWA group, 246 mRNAs were considerably upregulated, while 12 mRNAs were significantly downregulated (Fig. 2B). According to the results of the matching KEGG analysis, the majority of differentially expressed genes were enriched in the Chemokine signaling pathway, Cytokine-cytokine receptor internation, and Viral protein interaction with cytokine and cytokine receptor (Fig. 2C, D). KEGG enrichment cycle diagram showed that differential gene enrichment of the top 20 pathways (Fig. 2E). KEGG-enriched bar chart show differential genes associated with signal transduction (Fig. 2F). GSEA-go and kegg suggest that iMWA is associated with the chemokine acivity, Cytokine-cytokine receptor interaction and Chemokine signalling pathway (Figure S2A–C). The chemokine pathway is important in mediating cellular signal transduction [18]. These results suggest that iMWA activates chemokine pathways.

To further investigate the correlation between iMWA and chemokines, we detected the key chemokines and receptors based on RNA sequencing results using qRT-PCR and ELISA, mainly including CCL2, CCL5, CXCL2, CXCL5, CCR2, CXCR2 and CCR5. The results showed that chemokine CXCL5 and chemoreceptor CXCR2 were significantly increased in iMWA-treated groups (Fig. 3A–C). The results suggested that iMWA treatment caused increased levels of CXCL5 and CXCR2, which in turn affected the HCC tumor immune microenvironment.

Changes of TIME after iMWA treatment in HCC mice model based on mass cytometry

To assess the effect of iMWA on the overall TIME of HCC, we measured the expression of the respective immune cell populations in the Ctrl group and the iMWA-treated group using mass cytometry. We cycled single, live, and intact CD45+ immune cells from the selected cells in the respective tissues. All samples showed clustering and subgroup annotation of CD45+ immune cells. There were 32 cell clusters in total, and we defined the respective cell cluster based on the specific markers of the respective cell type (Fig. 4A, B, Figure S1). Results showed that relative to Ctrl group, iMWA-treated led to decreased CD4+

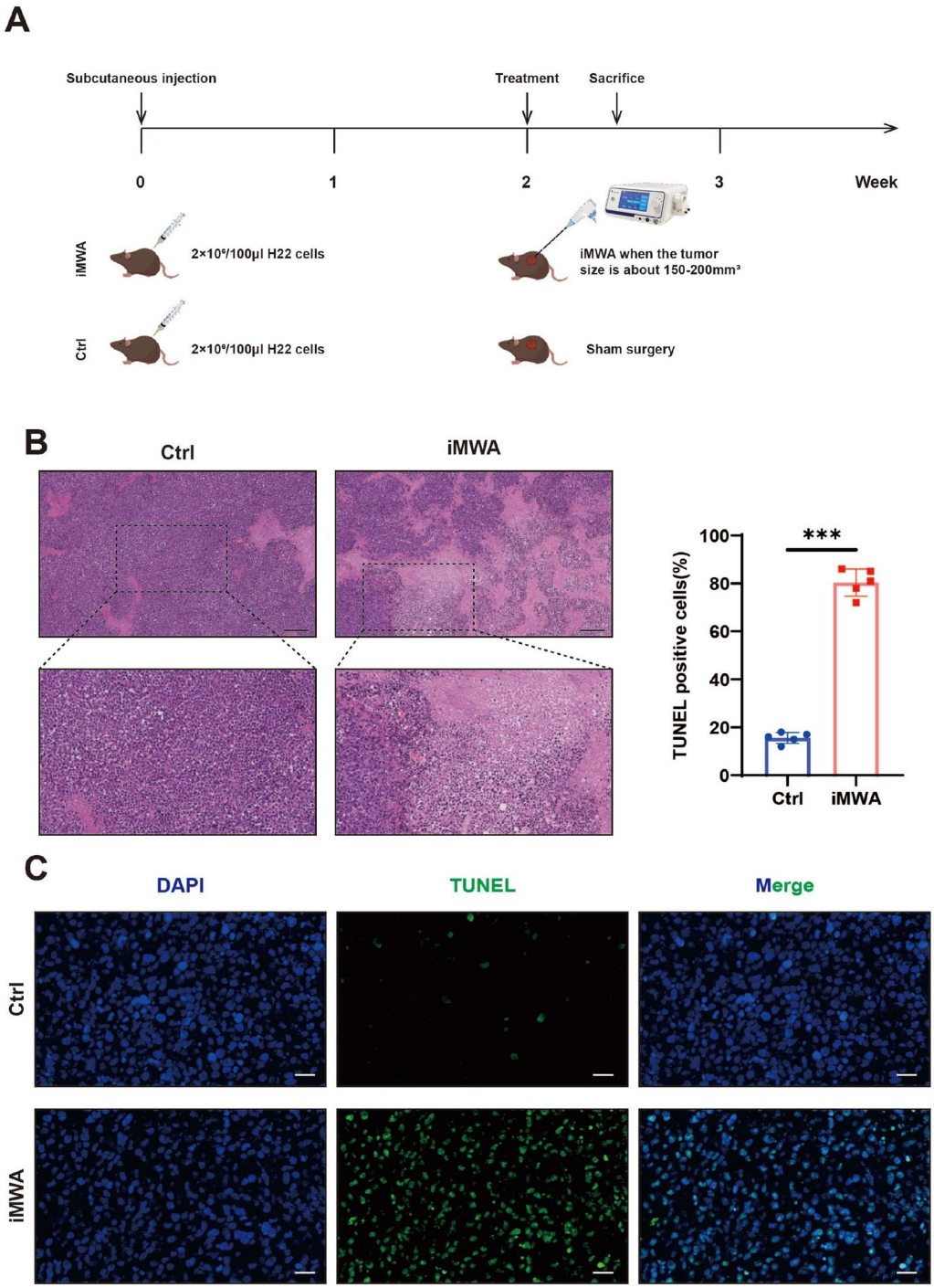

Fig. 1 Incomplete microwave ablation causes coagulative necrosis and apoptosis of cells in the ablation area. **A** Schematic diagram of experimental mice treatment. Mice were injected subcutaneously with H22 cells and treated with sham-operated (Ctrl) or iMWA (~ 50% ablation) 2 weeks later, and were executed 3 days after treatment. **B** H&E staining of tumor tissues on Ctrl and iMWA group after iMWA treatment, Scale bar, 200 μm. **C** TUNEL immunofluorescence detection of cell apoptosis at the ablation site of tumors after iMWA treatment. Scale bar, 20 μm.*P < 0.05; **P < 0.01; ***P < 0.001

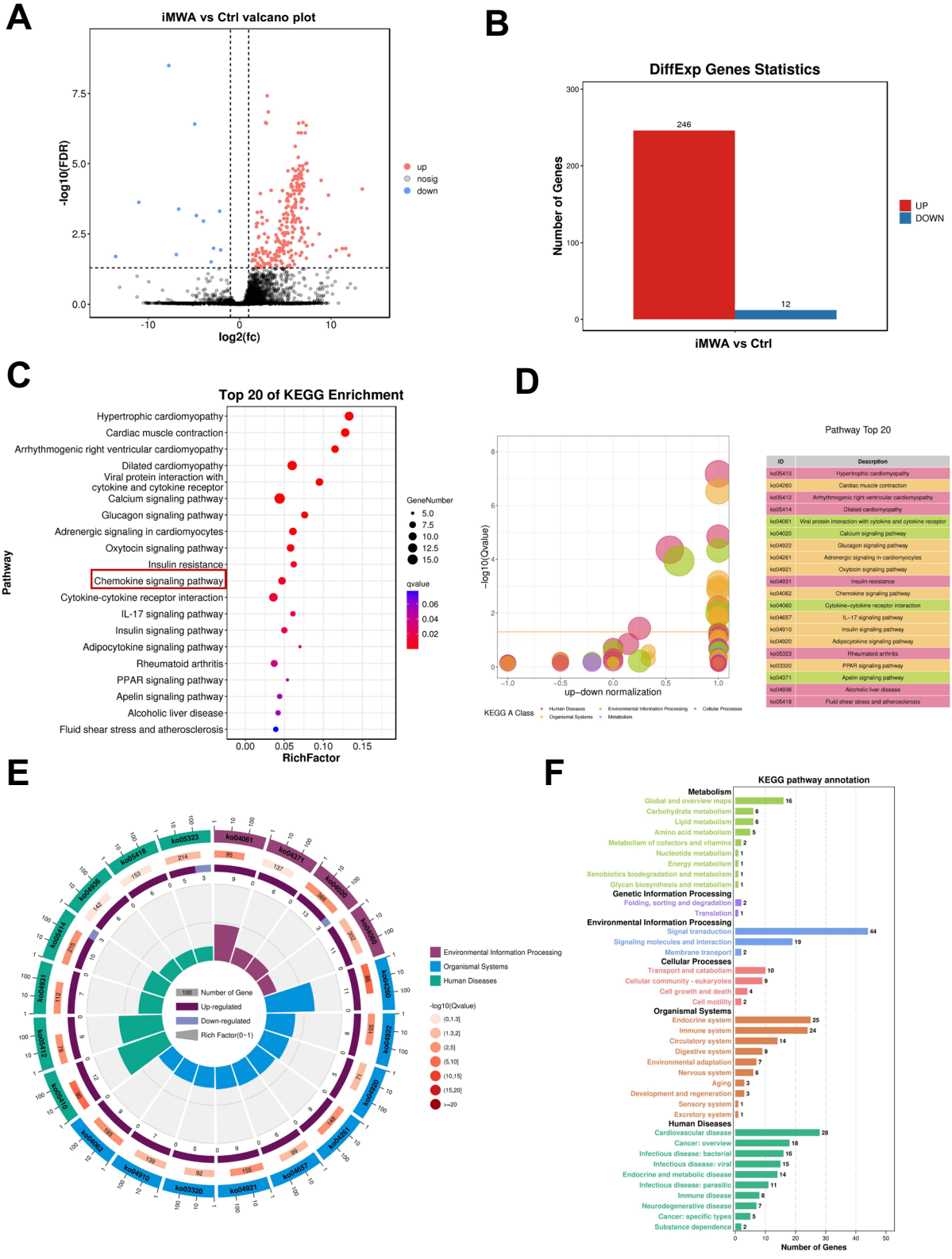

Fig. 2 iMWA induces chemokine alterations in the HCC tumor microenvironment. **A** Volcanic maps showing changes in gene expression after the iMWA in HCC. **B** Statistical map of up-regulated or down-regulated differential genes. **C**–**E** The enrichment of KEGG pathways among differentially expressed genes. **F** Differential gene KEGG enriched bar chart

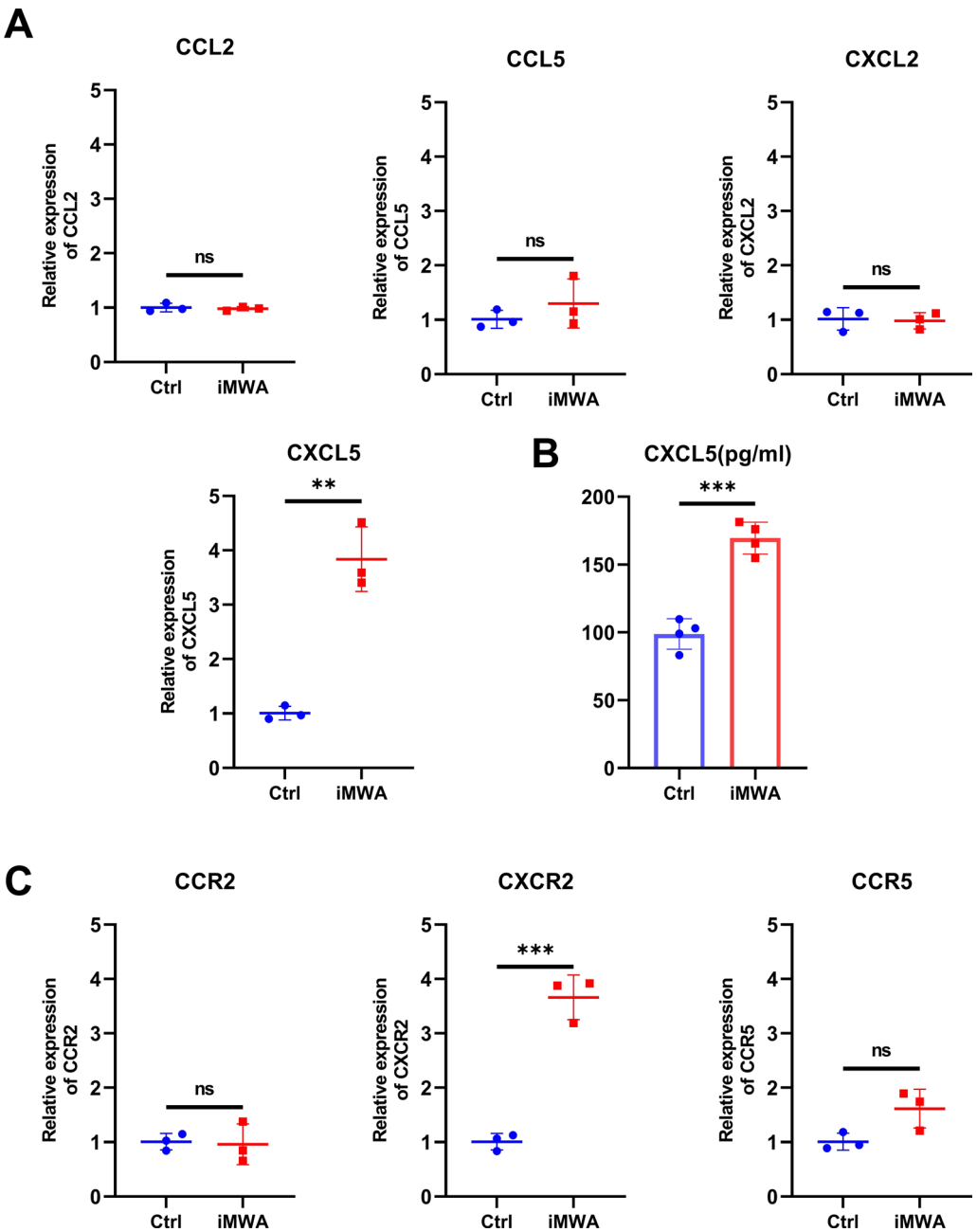

Fig. 3 iMWA increases CXCL5 levels in mouse HCC tumor tissues and peripheral blood. **A** qRT-PCR analysis of CCL2, CCL5, CXCL2 and CXCL5 in HCC tissues of C57BL/6 mice after iMWA. **B** ELISA detection of CXCL5 levels in peripheral blood of iMWA-treated HCC tumor-bearing C57BL/6 mice. **C** qRT-PCR analysis of CCR2, CXCR2 and CCR5 in HCC tissues of C57BL/6 mice after iMWA.*P < 0.05; **P < 0.01; ***P < 0.001

T, CD8+ T, Natural killer (NK), macrophages including both M1 and M2 types but increased monocytes and bone marrow-derived suppressor cells (MDSC) (Fig. 4C, D). In addition, we also analyzed the changes in the proportion of different cell populations compared to the total cell population, and the results showed the same trend, most notably a decrease in T, NK, and macrophages cells but an increase in MDSC cells in the iMWA-treated group (Fig. 4E). In particular, we showed that the C15 group is the MDSC group, which is highly enriched in iMWA-treated tissues, but the C17 group is the CD8+ T cell group, which is significantly reduced in iMWA-treated tissues (Fig. 5A, B). In order to further study the effect of iMWA group

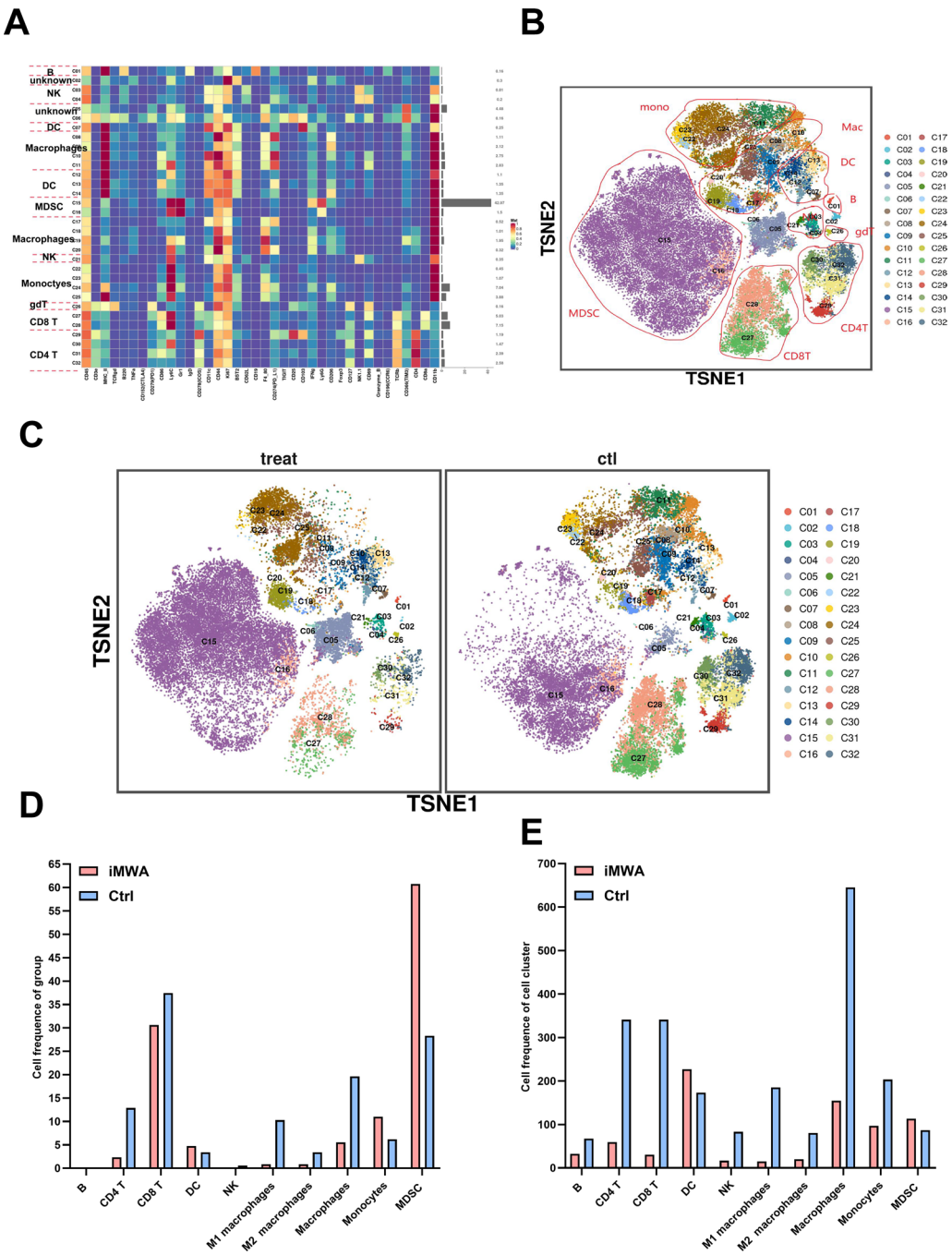

Fig. 4 Mass cytometry reflected the immune microenvironment of subcutaneous H22 tumors after iMWA treatment. **A** There were 32 cell clusters in total, which were defined in the respective groups. **B** TSNE plot showing distributions of 32 cell clusters. **C** TSNE diagram showing the distribution of cell clusters in the respective sample. **D** The bar chart showing the number of typical cell groups in each tissue. **E** The bar chart showing the number of typical cell populations in total population.*P < 0.05; **P < 0.01; ***P < 0.001

on MDSC, we used immunofluorescence staining of mouse tumor tissue in each group and found that the merged expressions of CD11b and Gr-1 proteins were higher in the iMWA-treated group compared with the Ctrl group (Fig. 5C). Immunohistochemistry suggested that CD8 was enriched in the control group but not in the iMWA-treated group (Fig. 5D).

We synchronously analyzed the detailed expression of some signature proteins in different groups. Results revealed that iMWA-treated group led to decreased CD8

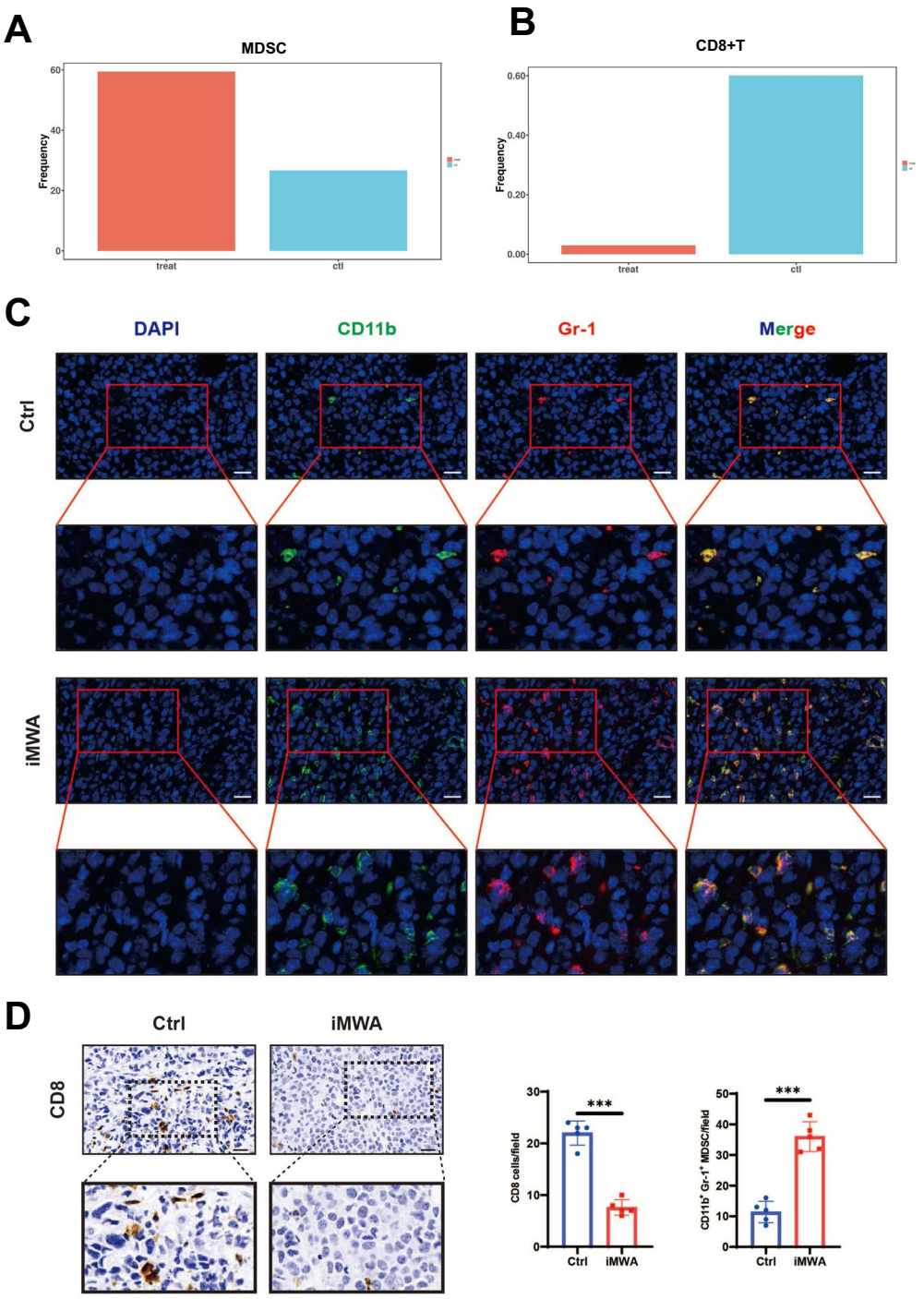

Fig. 5 Immunohistochemical and fluorescence results in different groups. **A** The histogram showing the number of MDSC in the respective sample based on mass cytometry. **B** The histogram showing the number of CD8 T in the respective sample based on mass cytometry. **C** Immunofluorescence of CD11b and Gr-1 in two groups, Scale bar, 20 μm. **D** Immunohistochemistry of CD8 in two groups, Scale bar, 20 μm.*P < 0.05; **P < 0.01; ***P < 0.001

and CD4 expression but increased TNFa, IFNg, and Gr-1 expression, which was assessed from the expression of the population sample (Fig. 6A–E). These results suggest that the iMWA group has a greater effect on TIME, especially the upregulation of MDSC and downregulation of CD8 T cells. MDSC express receptors such as CXCR2 and can be converted by CXCL5 secreted by tumor cells [19]. Combined with the results of RNA sequencing and qRT-PCR, we hypothesized that iMWA chemotaxis MDSC by increasing the level of CXCL5 in the HCC tumor microenvironment, which in turn induces accumulation.

iMWA and Gr-1 blocking combined therapy further inhibits HCC growth

Based on the previous conclusions, including the increase in chemokines, MDSC and decrease in CD8 T caused by iMWA, we searched the literature and found that these chemokines can recruit MDSC, and the increase of MDSC inhibits CD8 T cells [20–23]. Therefore, inhibiting MDSC is the main target in the later stage of iMWA. We established a subcutaneous tumor bearing model of C57BL/6 mice using H22 cells. iMWA treatment was performed 2 weeks after tumor inoculation. Injection of anti-Gr-1 was started 3 days after iMWA and then once a week and anti-IgG was as a control (Fig. 7A). The results showed that the tumor volume and weight of iMWA+ anti-Gr-1 group were significantly reduced compared with iMWA+ anti-IgG group (Fig. 7B–D). In addition, we used immunofluorescence staining of mouse tumor tissue in each group and found that the merged expressions of CD11b and Gr-1 proteins were reduced in the iMWA+ anti-Gr-1 group compared with the iMWA+ anti-IgG group (Fig. 7E). Immunohistochemistry suggested that CD8 was enriched in the iMWA+ anti-Gr-1 group but not in the iMWA+ anti-IgG group (Fig. 7F). Ki67 was significantly down-regulated in the iMWA+ anti-Gr-1 group, suggesting the growth of the cancer cells was effectively controlled (Fig. 7G).

These results suggest that iMWA and Gr-1 blocking combined therapy can further inhibit HCC growth and significantly improve the CD8+ T cells in the mouse subcutaneous tumor model.

Discussion

MWA is based on dielectric heating, which occurs when an imperfect dielectric material is exposed to an alternating electromagnetic (EM) field [24]. A microwave field oscillates rapidly (2450 MHz = 2.45 billion times a second), rotating polar molecules, primarily water, that oscillate out of phase, so some EM energy is absorbed and changed to heat. During treatment, MWA produces EM waves around an insulated, electrically independent antenna. The majority of the heat is due to the excitement of polar water particles, whereas ionic polarization influences for a much smaller part of the generated heat [25, 26]. MWA has some theoretical benefits compared with RFA: the target to be treated can be larger because it produces a larger area of necrosis; the time of treatment is shorter; and MWA is less influenced by the defense of the neighboring tissues due to vaporization and charring, so as the heat-sink effect influences less the efficacy of treatment. Because of the EM nature of microwaves, MWA is not limited by tissue conductance, as the propagation of energy is not dependent on electrical tissues properties, unlike RFA treatment [27]. According to the literature, overall survival, local recurrence, complication rates, disease-free survival, and mortality in patients with HCC treated with MWA (compared with RFA) vary between 22 months for focal lesion >3 cm (vs. 21 months) and 50 months for focal lesion ≤ 3 cm (vs. 27 months), between 5% (vs. 46.6%) and 17.8% (vs. 18.2%), between 2.2% (vs. 0%) and 61.5% (vs. 45.4%), between 14 months (vs. 10.5 months) and 22 months (vs. no data reported), and between 0% (vs. 0%) and 15% (vs. 36%), respectively [27]. Baker et al. assessed safety and efficacy of MWA in 340 patients with HCC. Median value of lesion size was 3.2 cm (range, 1–6). A total of 89.5% of patients had cirrhosis, 60.7% related to hepatitis C, and 8.2% related to hepatitis B. Slightly over one third (35.9%) were Child-Pugh class B/C cirrhotic. Laparoscopic MWA procedures were performed in 96.8% of the patients. Four patients died within 30 days (1.8%). Clavien–Dindo grade III complications happened in 3.2% of patients. Complete necrosis was recognized in 97.1% of tumors, whereas local recurrence was 8.5% at 10.9 months median follow-up (0–80 months). Local recurrence happened in 34.8% of patients at 10.9 months median follow-up, and metastatic recurrence rate was appreciated in 8.1% of patients. At 1 year, OS was 80.0%, whereas at 2 years OS was 61.5%. The researchers established that MWA could be performed safely, even in patients with advanced disease. The minimally invasive procedure determines low morbidity and mortality with acceptable incomplete necrosis rates and regional recurrence [28].

As one of the commonly used thermal ablation techniques, some recent studies have reported the effect of RFA on the immune microenvironment of HCC. The peripheral blood levels of CD4+ T cells, CD4+ CD8+ T cells, and CD4+ CD25+ CD127+ Tregs were significantly higher and levels of CD16+ CD56+ natural killer cells were significantly lower in HCC patients after RFA [29]. RFA promoted the release of large amounts of HSP-70 in the serum leading to local inflammation and activation of antigen-presenting cells in the tumor region [30]. Thermal ablation-mediated upregulation of METTL1

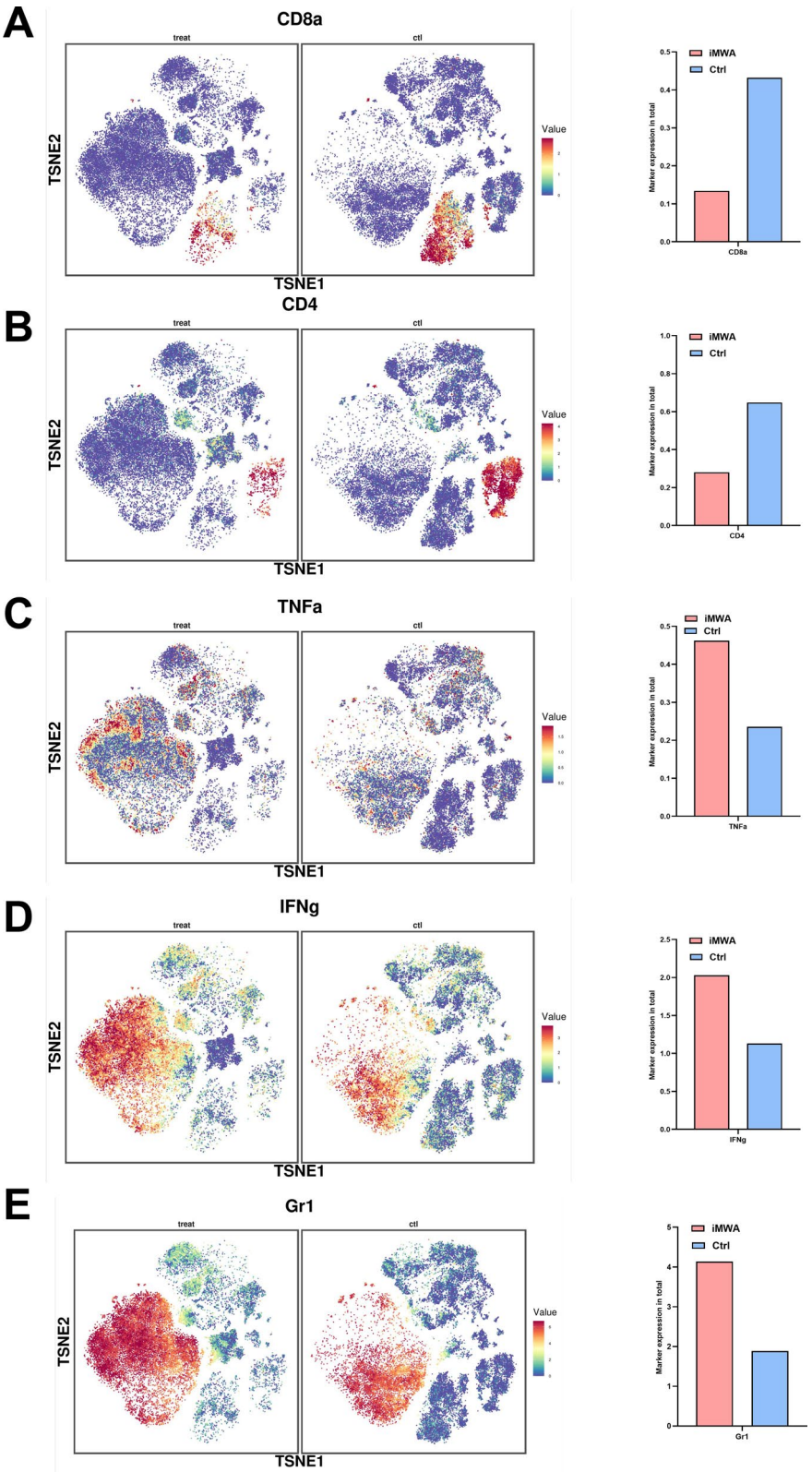

Fig. 6 Specific marker changes after iMWA treatment in HCC mice model based on mass cytometry. **A**–**E** TSNE plot showing the distribution of some markers. *P < 0.05; **P < 0.01; ***P < 0.001

enhanced TGF-β2 translation by inducing MDSC to create an immunosuppressive environment [31]. In addition, studies have shown that thermal ablation remodels the HCC immune microenvironment by affecting cytokine expression levels. Inflammatory cytokines such as IL-1β, IL-6, and TNF-α are more expressed after RFA, inducing enhanced immune response in HCC [32]. After RFA, the expression of immunosuppressive cytokines such as IL-10, TGF-β secreted in the HCC tumor microenvironment was reduced. In contrast, IFN-γ levels increased after RFA [33].

Changes in circulating immune cells/factors and TIME have been explored by analyzing peripheral blood and tumor models. Studies have shown that in the tumor model established by 4T1 breast cancer cells, MWA can activate T cell immune response, and MWA-based combination therapy can significantly induce th1 type anti-tumor response [34]. MWA combined with TIGIT blocking has a synergistic anticancer effect [35]. LAG3 blocking combined with MWA can reprogram TIME into an anti-tumor mode by promoting the function of CD8+ TIL [36]. Following thermal ablation, Katharina Leuchte et al. examined tumor-specific immune responses in the peripheral blood of HCC patients in relation to T cell responses and prognosis. While fluorospot analyses of specific T cell responses against seven tumor-associated antigens (TTAs) revealed de-novo or enhanced tumor-specific immune responses in 30% of patients, comprehensive flow cytometric analyses in sequential samples of a prospective patient cohort (n = 23) revealed only moderate effects of MWA on circulating immune cell subsets. The presence of tumor-specific T cell responses (IFN-y and/or IL-5) was linked to longer progression-free survival (27.5 vs. 10.0 months), and interferon-y and interleukin-5T cell responses against TAAs were more common in patients with a long-term remission (> 1 year) after MWA (7/16) compared to patients suffering from an early relapse (0/13 patients). These findings suggest that the anti-tumor immune response is related to tumor control. In patients getting combined MWA and resection, digital image analysis of immunohistochemically stained archival HCC tissues (n = 18) showed that individuals with high T cell abundance at the time of thermal ablation had a greater disease-free survival (37.4 vs. 13.1 months). Their data demonstrates remarkable immune-related effects of MWA in HCC patients and provides additional evidence for a combination of local ablation and immunotherapy in this challenging disease [37]. However, all the above studies focused on the influence of peripheral immunity after MWA, rather than the influence of the microenvironment of tumor tissue itself. However, our study adopted incomplete MWA to detect the change of TIME, which is of pioneering significance.

In our study, RNA sequencing analyses of HCC mouse models demonstrated that iMWA promotes the production of chemokines. To validate these results, qRT-PCR analysis revealed a significant increase in the expression of chemokine CXCL5 and chemokine receptor CXCR2 in the iMWA group. Elevated chemokine CXCL5 has been reported to be strongly associated with the recruitment of MDSCs and suppression of CD8+ T-cells. In contrast, the chemokine receptor CXCR2, which is highly expressed in gMDSC, mediates MDSC aggregation, reduces CD8+ T-cell infiltration, and suppresses the activation of anti-tumour T-cell immunity, ultimately leading to tumour progression and immune escape [38, 39]. Mass spectrometry analysis showed that iMWA treatment caused a decrease in CD4+ T cells, CD8+ T cells, NK cells, and macrophages (both M1 and M2 types), but an increase in monocytes and MDSCs, compared with untreated controls. In terms of innate immunity, MDSCs inhibit the function of NK cells by downregulating the expression of NKG2D through membrane-bound TGF-β. Additionally, MDSCs also induce Treg amplification and promote their negative regulatory effect on immunity. In terms of adaptive immunity, MDSCs can competitively deplete cysteine in the body's environment and upregulate iNOS and Arg-1 activity, thereby depleting L-arginine. MDSCs can also inhibit T-cell immune responses by generating reactive oxygen species (ROS) [40, 41]. The findings of our study demonstrate that MDSCs play a significant role in the heightened risk of short-term tumour recurrence observed in the iMWA subgroup. To gain further insight into the impact of iMWA on MDSCs, immunofluorescence staining of tumour tissues from mice in each group was performed, which revealed a higher co-expression of CD11b and Gr-1 proteins in the iMWA group compared with the control group. Immunohistochemical staining

(See figure on next page.)

Fig. 7 Specific effects of iMWA and Gr-1 blocking combined therapy in HCC mouse model. **A** Schematic diagram of treatment of experimental mice. Mice were injected subcutaneously with H22 cells and treated with sham operation (Ctrl) or iMWA (~ 50% ablation) after 2 weeks. After ablation, they received anti-IgG or Gr-1 treatment once a week and were executed at week 4. **B** Representative images of tumors from nude mice in two groups. **C**, **D** Tumor growth curves and tumor weights of each group. **E** Immunofluorescence of CD11b and Gr-1 in two groups, Scale bar, 20 μm. **F** Immunohistochemistry of CD8 in two groups, Scale bar, 20 μm. **G** The expression level of Ki67 in nude mice-derived xenograft tumor was determined by Immunofluorescence, Scale bar, 20 μm. *P < 0.05; **P < 0.01; ***P < 0.001

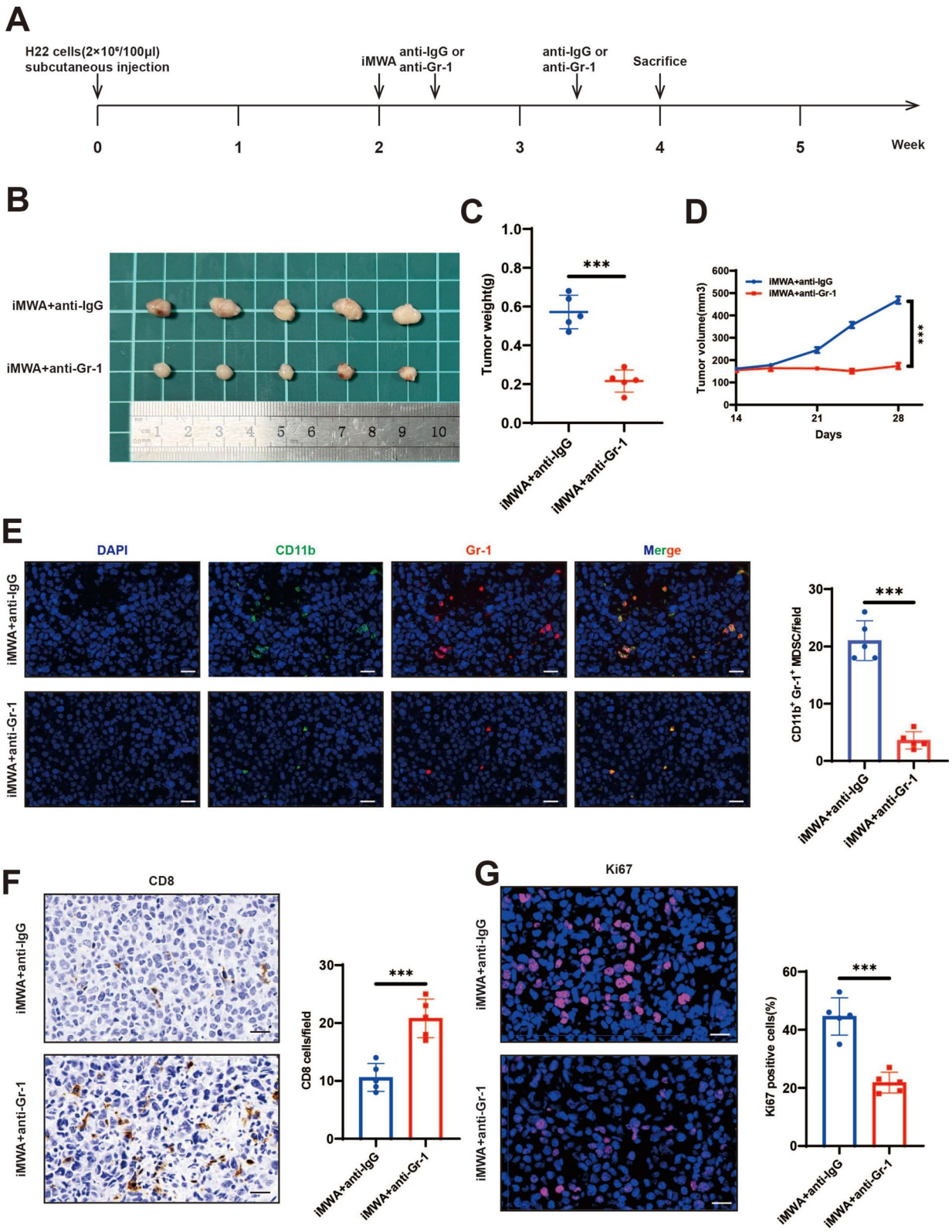

Fig. 7 (See legend on previous page.)

further showed that CD8+ T-cell infiltration was abundant in the control group but not in the iMWA-treated group. A study reported that Gr-1 monoclonal antibody can be used to inhibit the recruitment of MDSC [42]. To validate this finding, we began injecting anti-Gr-1 into hormonal mice after 3 days of iMWA treatment. Solid tumour regression results showed a significant reduction in tumour volume and weight in the iMWA+ anti-Gr-1 group compared with the iMWA+ anti-IgG group. Immunohistochemistry additionally showed a re-enrichment of CD8+ T-cells and a significant down-regulation of Ki67 in the iMWA+ anti-Gr-1 group, indicating that Gr-1 monoclonal antibody effectively controlled cancer cell growth. Our study thereby illuminates the MDSC recruitment through the CXCL5-CXCR2 axis in the iMWA group and that this phenomenon can be reversed by Gr-1 monoclonal antibody.

Conclusion

To sum up, thermal stress generated by iMWA induces coagulative necrosis and apoptosis in the region of the ablation center of HCC. iMWA can boost chemokine CXCL5 and led to decreased CD4+ T, CD8+ T, NK, macrophages including both M1 and M2 types but increased monocytes and MDSC. iMWA and Gr-1 blocking combined therapy can further inhibit HCC growth and significantly improve the CD8+ T cells in the mouse subcutaneous tumor model, which brings good news to HCC patients.

Supplementary Information

The online version contains supplementary material available at https://doi.org/10.1186/s12935-024-03578-w.

Supplementary Material 1.

Supplementary Material 2.

Acknowledgements
Not applicable.

Author contributions
There are 3 first authors in this manuscript and they have equally contributed to this project. Dr. TH, HSC and SPD were responsible for performing the experiments as well as drafting the manuscript. Dr. YHZ, HYL, SXZ, ZQL and CL performed part of the experiments and interpreted the data. Furthermore, we have 4 corresponding authors in this manuscript. Dr. CYL, ZXL, JHS and HZ have contributed to design the study and critical revised the manuscript. All authors read and approved the final manuscript. We would like to thank the Core Facility of the First Affiliated Hospital of Nanjing Medical University for its help in the experiment.

Funding
This work was supported by grants from the National Natural Science Foundation of China (82372065), Clinical capacity improvement engineering medical project (JSPH-MC-2022-30), National Natural Science Foundation Youth Fund cultivation program (PY2023057), National Natural Science Foundation Youth Fund cultivation program(PY2023057), Clinical capacity improvement engineering medical project (JSPH-MC-2022-30) from The First Affiliated Hospital of Nanjing Medical University, Nanjing Major Science and Technology Project (202305044), and sponsored by Shanghai Pujiang Program (23PJ1407400).

Availability of data and materials
The authors declare that all data supporting the results in this study are available within the paper and its supplementary information. Source data for the figures in this study are available from the corresponding author upon reasonable request.

Declarations

Ethics approval and consent to participate
All in vivo animal experiments were approved by the Committee on the Ethics of Animal Experiments of Nanjing Medical University.

Consent for publication
Not applicable.

Competing interests
The authors declare no competing interests.

Author details
[1]Hepatobiliary Center, The First Affiliated Hospital of Nanjing Medical University, Key Laboratory of Liver Transplantation, Chinese Academy of Medical Sciences, NHC Key Laboratory of Hepatobiliary Cancers, Nanjing, China. [2]Department of General Surgery, Nanjing First Hospital, Nanjing Medical University, Nanjing, China. [3]Canyon Medical Inc., Nanjing, Jiangsu, China. [4]Department of Plastic and Reconstructive Surgery, Shanghai Ninth People's Hospital, Shanghai Jiao Tong University School of Medicine, Shanghai, China. [5]Center of Interventional Radiology & Vascular Surgery, Department of Radiology, Zhongda Hospital, Medical School, Southeast University, Nanjing, China.

Received: 9 November 2023 Accepted: 19 November 2024
Published online: 04 December 2024

References

1. Sung H, Ferlay J, Siegel RL, et al. Global cancer statistics 2020: GLOBOCAN estimates of incidence and mortality worldwide for 36 cancers in 185 countries. CA Cancer J Clin. 2021;71(3):209–49.
2. Forner A, Reig M, Bruix J. Hepatocellular carcinoma. Lancet. 2018;391(10127):1301–14.
3. Allemani C, Weir HK, Carreira H, et al. Global surveillance of cancer survival 1995–2009: analysis of individual data for 25,676,887 patients from 279 population-based registries in 67 countries (CONCORD-2). Lancet. 2015;385(9972):977–1010.
4. Torre LA, Bray F, Siegel RL, et al. Global cancer statistics, 2012. CA Cancer J Clin. 2015;65(2):87–108.
5. Dai S, Zhao W, Yue L, et al. A competing risk for nomogram of the role of metastasectomy in patients with colorectal cancer and liver metastases. Asian J Surg. 2023;46(6):2468–71.
6. Zhou M, Wang H, Zeng X, et al. Mortality, morbidity, and risk factors in China and its provinces, 1990–2017: a systematic analysis for the Global Burden of Disease Study 2017. Lancet. 2019;394(10204):1145–58.
7. Huang J, Yan L, Cheng Z, et al. A randomized trial comparing radiofrequency ablation and surgical resection for HCC conforming to the Milan criteria. Ann Surg. 2010;252(6):903–12.
8. Takayama T, Hasegawa K, Izumi N, et al. Surgery versus radiofrequency ablation for small hepatocellular carcinoma: a randomized controlled trial (SURF Trial). Liver Cancer. 2022;11(3):209–18.
9. Bruix J, Sherman M. Management of hepatocellular carcinoma. Hepatology. 2005;42(5):1208–36.
10. Ahmed M, Brace CL, Lee FT Jr, et al. Principles of and advances in percutaneous ablation. Radiology. 2011;258(2):351–69.
11. Yu NC, Raman SS, Kim YJ, et al. Microwave liver ablation: influence of hepatic vein size on heat-sink effect in a porcine model. J Vasc Interv Radiol. 2008;19(7):1087–92.

12. Schramm W, Yang D, Wood BJ, et al. Contribution of direct heating, thermal conduction and perfusion during radiofrequency and microwave ablation. Open Biomed Eng J. 2007;1:47–52.
13. Copper IS. Cryogenic surgery: a new method of destruction or extirpation of benign or malignant tissues. N Engl J Med. 1963;268:743–9.
14. Jungraithmayr W, Burger D, Olschewski M, et al. Cryoablation of malignant liver tumors: results of a single center study. Hepatobiliary Pancreat Dis Int. 2005;4(4):554–60.
15. Lv B, Wang Y, Ma D, et al. Immunotherapy: reshape the tumor immune microenvironment. Front Immunol. 2022;13: 844142.
16. Darvin P, Toor SM, Sasidharan Nair V, et al. Immune checkpoint inhibitors: recent progress and potential biomarkers. Exp Mol Med. 2018;50(12):1–11.
17. Zheng Z, Ma M, Han X, et al. Idarubicin-loaded biodegradable microspheres enhance sensitivity to anti-PD1 immunotherapy in transcatheter arterial chemoembolization of hepatocellular carcinoma. Acta Biomater. 2022;157:337–51.
18. Miyajima A, Kitamura T, Harada N, et al. Cytokine receptors and signal transduction. Annu Rev Immunol. 1992;10:295–331.
19. Zhao J, Ou B, Han D, et al. Tumor-derived CXCL5 promotes human colorectal cancer metastasis through activation of the ERK/Elk-1/Snail and AKT/GSK3β/β-catenin pathways. Mol Cancer. 2017;16(1):70.
20. Chen Y, Kim J, Yang S, et al. Type I collagen deletion in αSMA(+) myofibroblasts augments immune suppression and accelerates progression of pancreatic cancer. Cancer Cell. 2021;39(4):548-65.e6.
21. Chang M, He Y, Liu C, et al. Downregulation of SEPTIN5 inhibits prostate cancer progression by increasing CD8(+) T cell infiltration. Int J Biol Sci. 2022;18(16):6035–51.
22. Chen H, Pan Y, Zhou Q, et al. METTL3 inhibits antitumor immunity by targeting m(6)A-BHLHE41-CXCL1/CXCR2 axis to promote colorectal cancer. Gastroenterology. 2022;163(4):891–907.
23. Cheng Y, Mo F, Li Q, et al. Targeting CXCR2 inhibits the progression of lung cancer and promotes therapeutic effect of cisplatin. Mol Cancer. 2021;20(1):62.
24. Simon CJ, Dupuy DE, Mayo-Smith WW. Microwave ablation: principles and applications. Radiographics. 2005;25(Suppl 1):S69-83.
25. Tanaka M, Sato M. Microwave heating of water, ice, and saline solution: molecular dynamics study. J Chem Phys. 2007;126(3): 034509.
26. Liang P, Yu J, Lu MD, et al. Practice guidelines for ultrasound-guided percutaneous microwave ablation for hepatic malignancy. World J Gastroenterol. 2013;19(33):5430–8.
27. Izzo F, Granata V, Grassi R, et al. Radiofrequency ablation and microwave ablation in liver tumors: an update. Oncologist. 2019;24(10):e990–1005.
28. Felsher J, Chand B, Ponsky J. Minimally invasive surgery. Endoscopy. 2003;35(2):171–7.
29. Shi ZR, Duan YX, Cui F, et al. Integrated proteogenomic characterization reveals an imbalanced hepatocellular carcinoma microenvironment after incomplete radiofrequency ablation. J Exp Clin Cancer Res. 2023;42(1):133.
30. Haen SP, Gouttefangeas C, Schmidt D, et al. Elevated serum levels of heat shock protein 70 can be detected after radiofrequency ablation. Cell Stress Chaperones. 2011;16(5):495–504.
31. Zeng X, Liao G, Li S, et al. Eliminating METTL1-mediated accumulation of PMN-MDSCs prevents hepatocellular carcinoma recurrence after radiofrequency ablation. Hepatology. 2023;77(4):1122–38.
32. Ahmad F, Gravante G, Bhardwaj N, et al. Changes in interleukin-1β and 6 after hepatic microwave tissue ablation compared with radiofrequency, cryotherapy and surgical resections. Am J Surg. 2010;200(4):500–6.
33. Huang KW, Jayant K, Lee PH, et al. Positive immuno-modulation following radiofrequency assisted liver resection in hepatocellular carcinoma. J Clin Med. 2019;8(3):385.
34. Li L, Wang W, Pan H, et al. Microwave ablation combined with OK-432 induces Th1-type response and specific antitumor immunity in a murine model of breast cancer. J Transl Med. 2017;15(1):23.
35. Chen Y, Huang H, Li Y, et al. TIGIT blockade exerts synergistic effects on microwave ablation against cancer. Front Immunol. 2022;13: 832230.
36. Shao D, Chen Y, Huang H, et al. LAG3 blockade coordinates with microwave ablation to promote CD8(+) T cell-mediated anti-tumor immunity. J Transl Med. 2022;20(1):433.
37. Leuchte K, Staib E, Thelen M, et al. Microwave ablation enhances tumor-specific immune response in patients with hepatocellular carcinoma. Cancer Immunol Immunother. 2021;70(4):893–907.
38. Fujimura T, Aiba S. Significance of immunosuppressive cells as a target for immunotherapies in melanoma and non-melanoma skin cancers. Biomolecules. 2020;10(8):1087.
39. Korbecki J, Kupnicka P, Chlubek M, et al. CXCR2 receptor: regulation of expression, signal transduction, and involvement in cancer. Int J Mol Sci. 2022;23(4):2168.
40. Yang T, Li J, Li R, et al. Correlation between MDSC and immune tolerance in transplantation: cytokines, pathways and cell-cell interaction. Curr Gene Ther. 2019;19(2):81–92.
41. Zhang J, Fan J, Zeng X, et al. Hedgehog signaling in gastrointestinal carcinogenesis and the gastrointestinal tumor microenvironment. Acta Pharm Sin B. 2021;11(3):609–20.
42. Xie M, Lin Z, Ji X, et al. FGF19/FGFR4-mediated elevation of ETV4 facilitates hepatocellular carcinoma metastasis by upregulating PD-L1 and CCL2. J Hepatol. 2023;79(1):109–25.

Publisher's Note